JACS
JOURNAL OF THE AMERICAN CHEMICAL SOCIETY
Article
pubs.acs.org/JACS

A Flexible Microporous Hydrogen-Bonded Organic Framework for Gas Sorption and Separation

Hailong Wang,[†] Bin Li,[†] Hui Wu,[‡] Tong-Liang Hu,[†] Zizhu Yao,[§] Wei Zhou,*[,‡] Shengchang Xiang,[§] and Banglin Chen*[,†]

[†]Department of Chemistry, University of Texas at San Antonio, San Antonio, Texas 78249-0698, United States

[‡]NIST Center for Neutron Research, National Institute of Standards & Technology, Gaithersburg, Maryland 20899-6102, United States

[§]College of Material Science and Engineering, Fujian Provincial Key Laboratory of Polymer Materials, Fujian Normal University, 32 Shangsan Road, Fuzhou 350007, China

Supporting Information

ABSTRACT: A microporous three-dimensional hydrogen-bonded organic framework (HOF-5) has been constructed from a new organic linker 4,4′,4″,4‴-tetra(2,4-diamino-1,3,5-triazin-6-yl)tetraphenylethene. Activated HOF-5a exhibits a stepwise N_2 adsorption isotherm at 77 K, suggesting framework flexibility. The structure of activated HOF-5a has been established by powder X-ray diffraction studies, indicating a significant framework contraction from as-synthesized HOF-5 to activated HOF-5a of ∼21% by volume. HOF-5a shows moderately high porosity with a Brunauer−Emmett−Teller (BET) surface area of 1101 m^2/g, and takes up a large amount of acetylene and carbon dioxide under ambient conditions. Powder neutron diffraction studies and theoretical calculations reveal that suitable pore sizes, curvatures, and functional sites collectively enable HOF-5a to encapsulate a high density of carbon dioxide molecules packed in a pseudo-one-dimensional array along the pore channel.

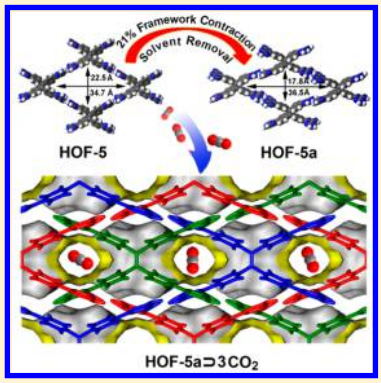

INTRODUCTION

Over the years, research on porous media, from traditional zeolites, carbons, and mesoporous materials to metal−organic frameworks (MOFs) and covalent-organic frameworks (COFs), has demonstrated the crucial roles of such materials for the advancement of science and technology.[1−5] The extensive pursuit of MOFs and COFs over the past two decades has not only led to new porous materials that can mimic traditional zeolites and porous carbons, but has also generated a number of novel materials with superior properties, thus rendering them promising for gas storage/separation, sensing, heterogeneous catalysis, and biomedical applications.[3−5]

Compared with MOFs and COFs, which are self-assembled through coordination and covalent bonding of their corresponding building units, the hydrogen-bonded organic frameworks (HOFs), self-assembled frameworks through weaker hydrogen bonding interactions among molecular organic linkers, are much more fragile and difficult to stabilize.[6,7] It is therefore not surprising that research on HOFs has been significantly lagging behind that of MOFs and COFs, although the concepts to construct MOFs and HOFs were basically proposed during the same period around the early 1990s.

Recently, there has been a renewed interest in the exploration of porous HOFs.[8,9] This is because HOFs can be easily synthesized and characterized. Furthermore, the more straightforward processing and facile recycling (simply through recrystallization) have enabled them to be particularly useful for device implementation.[10] Some progress has been made to stabilize HOFs and thus to establish permanent porosities. Until now, a dozen HOFs have been discovered to display permanent porosities as confirmed by vapor/gas sorption isotherms.[8,9] A few of them even exhibit properties superior to other porous materials for the separation of C_2H_2/C_2H_4,[9a] C_2H_2/CO_2,[9b] and fluororocarbons[8f] as well as chiral secondary alcohols,[9c] exemplifying the bright promise of HOFs as a new category of functional materials.

Although research on HOFs has been developed for quite a long time, those with both established permanent porosities by gas sorption isotherms and functional properties are still rare. Some in-depth systematical studies, including the exploration of new hydrogen bonding motifs, backbones, and organic linkers for the construction of HOFs and detailed crystallographic studies on framework robustness and flexibility, are certainly necessary before we can harness the rich chemistry of HOFs to rationally design and synthesize porous functional materials. By incorporating the well-known hydrogen bonding motif DAT (2,4-diaminotriazinyl group) with the tetraphenylethylene (TPE) backbone, we developed a new organic linker (L) (see Figure 1a) for the assembly of a novel HOF, which we named "HOF-5". Herein, we report the crystal structure of as-

Received: June 1, 2015
Published: July 27, 2015

ACS Publications © 2015 American Chemical Society

DOI: 10.1021/jacs.5b05644
J. Am. Chem. Soc. 2015, 137, 9963−9970

synthesized HOF-5, showing its microporous nature. HOF-5 framework was found to be quite flexible. Upon activation, the structure contracts significantly with a change in crystal symmetry, as revealed by powder X-ray diffraction studies. The resulting fully activated HOF-5a has a moderately high Brunauer–Emmett–Teller (BET) surface area of 1101 m^2/g, and exhibits quite interesting gas sorption behaviors, particularly for CO_2 capture and separation (CCS). The CO_2 uptake is ~90 cm^3/g (86 cm^3/cm^3) at 1 atm and 296 K, which is the highest value among all porous HOFs, and comparable to those very few MOFs and COFs exhibiting high performance for postcombustion CCS. The specific binding of HOF-5a for CO_2 molecules has been further established by neutron powder diffraction studies and density-functional theory (DFT) calculations.

EXPERIMENTAL SECTION

General Remarks. All reagents and solvents were used directly as received from the chemical supplier without further purification. The precursors, tetra(4-bromophenyl)ethylene and tetra(4-cyanophenyl)-ethylene, were prepared according to a slight modification of the reported procedures (Scheme 1).[11,12] During the preparation of this manuscript, this organic ligand was reported to assemble a nonporous hydrogen-bonded organic framework,[13] so the detailed synthesis of the organic ligand was provided in the Supporting Information.

Scheme 1. Schematic Synthesis of the Organic Linker L for the Self-Assembly of HOF-5

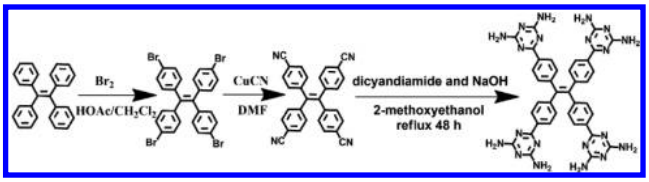

IAST Calculation. Adsorption isotherms and gas selectivities of mixed C_2H_2/CH_4 (50:50), CO_2/CH_4 (50:50), and CO_2/N_2 (10:90) at different temperatures were calculated based on the ideal adsorbed solution theory (IAST) proposed by Myers and Prausnitz.[14] In order to predict the sorption performance of this HOF toward the separation of binary mixed gases, the parameters fitted from the single-component C_2H_2, CO_2, CH_4, and N_2 adsorption isotherms based on the dual-site Langmuir–Freundlich (DSLF) model were used in the IAST calculations.[15] The fitting parameters of the DSLF equation are listed in Table S1.

Single Crystal and Powder X-ray Crystallography. Crystallographic data of an as-synthesized HOF-5 single crystal were collected on an Oxford Diffraction SuperNova diffractometer with Cu Kα radiation (λ = 1.54184 Å) at 100.00(16) K. Final unit cell parameters were derived from the global refinements of reflections obtained from the integration of all frame data. The collected frames were integrated using the preliminary cell-orientation matrix. CrysAlisPro Agilent Technologies software was used for collecting the frames of data, indexing the reflections, and determining the lattice constants, and SCALE3 ABSPACK software was utilized for the absorption correction. The structure was solved using the direct method (*SHELXS-97*) and refined utilizing full-matrix least-squares (*SHELXL-97*) on F^2.[16] Anisotropic thermal parameters were used for the nonhydrogen atoms and isotropic parameters for the hydrogen atoms. Hydrogen atoms were added geometrically and refined using a riding model. In addition, we note that the "SQUEEZE" command was employed because of the seriously disordered THF, DMF, and DMSO molecules in the HOF pores.

Powder X-ray diffraction (powder XRD) measurements were conducted on as-synthesized HOF-5 crystals in mother liquid, fully activated HOF-5a, and acetone regenerated HOF-5a, all sealed in glass capillaries, using a Rigaku Ultima IV diffractometer with Cu Kα radiation. The powder XRD pattern of activated HOF-5a sample can be indexed using a monoclinic system, and the space group was identified as $C2/m$. The structure was then solved using the direct method. Finally, Rietveld refinement was performed on the powder XRD pattern using the GSAS package.[18] Refinement on the lattice parameters, background, and peak profile, as well as the atomic positions of C and N with constraints applied on C–C and C–N bond lengths yielded the agreement factors of R_{wp} = 0.0625 and R_p = 0.0488, which strongly confirms the validity of our structure solution. The positions of H atoms were estimated from the geometry and the common length of C–H bonds of the benzene ring and N–H bonds of the primary amine. Selected crystallographic data and pertinent information for these two phases are summarized in Table 1. CCDC 1057513 and 1052041 for HOF-5 and HOF-5a, respectively, contain the supplementary crystallographic data for this paper. These data can be obtained free of charge from the Cambridge Crystallographic Data Centre via www.ccdc.cam.ac.uk/data_request/cif.

Table 1. Crystallographic and Refinement Parameters for HOF-5 and HOF-5a

crystal data	HOF-5	HOF-5a
system	monoclinic	monoclinic
space group	$C2/c$	$C2/m$
MF	$C_{38}H_{32}N_{20}$	$C_{38}H_{32}N_{20}$
FW	768.84	768.84
a/Å	21.6470(5)	14.3476(19)
b/Å	22.0832(5)	17.8692(21)
c/Å	14.1759(3)	12.2628(20)
α/^{o}	90	90
β/^{o}	92.692(2)	121.697(9)
γ/^{o}	90	90
volume/Å^3	6769.1(3)	2675.0(7)
Z	4	2
density/g/cm^3	0.754	0.955
solvent-accessible void space/%	55.3	41.1
theoretical pore volume/ cm^3/g	0.72[a]	0.43[a]
refinement parameters	R_1 = 0.0585[b] wR_2 = 0.1769[c]	R_{wp} = 0.0625 R_p = 0.0488

[a]Calculated on the basis of the HOF crystal structures using PLATON software.[17] [b]$R_1 = \Sigma||F_0| - |F_c||/\Sigma|F_0|$. [c]$wR_2 = [\Sigma w(F_0^2 - F_c^2)^2/\Sigma w(F_0^2)^2]^{1/2}$.

Neutron Diffraction Experiment. Powder neutron diffraction data were collected using the BT-1 neutron powder diffractometer at the National Institute of Standards and Technology (NIST) Center for Neutron Research. A Ge(311) monochromator with a 75° takeoff angle, λ = 2.0787(2) Å, and in-pile collimation of 60 min of arc was used. Data were collected over the range of 1.3–166.3° (2θ) with a step size of 0.05°. Fully activated HOF-5a sample was loaded in a vanadium can equipped with a capillary gas line and a packless valve. A closed-cycle He refrigerator was used for sample temperature control. The sample of activated HOF-5a was measured first at the temperatures of 6, 100, and 200 K. No phase transition was observed, indicating a relatively "robust" HOF-5a pore structure within this temperature range. To probe the preferential CO_2 adsorption locations, a predetermined amount of CO_2 (~1.5CO_2 per L molecule) was loaded into the sample at room temperature. The sample was then slowly cooled to 200 K before diffraction data were collected.

Rietveld structural refinement was also performed on the neutron diffraction data.[18] Due to the large incoherent background (mainly from the elemental H in HOF-5a), the overall data quality is modest, and thus both the HOF-5 building block (L) and CO_2 molecules were treated as rigid bodies in Rietveld refinement (to limit the number of variables), with the molecule orientation and center of mass freely

DOI: 10.1021/jacs.5b05644
J. Am. Chem. Soc. 2015, 137, 9963–9970

refined. Final refinement on the positions/orientations of the rigid bodies, thermal factors, occupancies, lattice parameters, background, and profiles converges with satisfactory *R*-factors.

Density-Functional Theory Calculations. First-principles density-functional theory (DFT) calculations were performed using the Quantum-Espresso package.[19] A semiempirical addition of dispersive forces to conventional DFT was included in the calculation to account for van der Waals interactions.[20] We used Vanderbilt-type ultrasoft pseudopotentials and generalized gradient approximation (GGA) with Perdew–Burke–Ernzerhof (PBE) exchange correlation. A cutoff energy of 544 eV and a 2 × 2 × 2 *k*-point mesh (generated using the Monkhosrt-Pack scheme) were found to be enough for the total energy to converge within 0.01 meV/atom. We first optimized the HOF-5a structure. The CO_2 gas molecule was then introduced to the optimized HOF structure at the experimentally identified adsorption site, followed by a full structural relaxation. To obtain the gas binding energy, a CO_2 gas molecule placed in a supercell with the same cell dimensions was also relaxed as a reference. The static binding energy (at T = 0 K) was then calculated using $E_B = E(\text{HOF-5a}) + E(CO_2) - E(\text{HOF-5a} \supset CO_2)$.

RESULTS AND DISCUSSION

Self-Assembly of HOF-5. The bromination reaction between tetraphenylethylene (TPE) and Br_2 in a mixed glacial acetic acid/dichloromethane solution yields tetra(4-bromophenyl)ethylene. Reaction time of 30 min is optimized on the basis of TLC detection (a longer reaction time led to the formation of unknown impurities). The corresponding organic linker L is obtained by the reaction of tetra(4-cyanophenyl)-ethylene with dicyandiamide in the presence of NaOH. HOF-5, as pale yellowish block-shaped single crystals, is self-assembled from organic linker L, through the slow diffusion of tetrahydrofuran (THF) into a DMF/DMSO (2:1) solution containing L at room temperature.

Crystal Structure of HOF-5. The single-crystal X-ray diffraction analysis at 100 K reveals that as-synthesized HOF-5 crystallizes in the monoclinic system and *C*2/*c* space group, and exhibits a microporous three-dimensional (3D) hydrogen-bonded structure. In the crystal structure of HOF-5, each organic linker is connected with eight neighboring organic linkers via 20 N–H···N hydrogen bonds between the 2,4-diaminotriazinyl (DAT) motifs. A two-dimensional (2D) supramolecular grid is achieved through the hydrogen bonds N4–H4A···N7#1 and N9–H9A···N2#4 (symmetry code #1: 1.5 − *x* + 3/2, 0.5 + *y*, 1.5 − *z* and #4: 1.5 − *x*, −0.5 + *y*, 1.5 − *z*), as shown in Figure S1. The hydrogen-bonded adjacent sheets are stacked in a repeated −[A–B–C]− staggered configuration through additional hydrogen bonding interactions to form the three-dimensional HOF-5. Topologically, we can consider the building linker L as a four-connected node and the center of neighboring six DAT motifs as a six-connected node to assemble into a hydrogen bonded organic framework net of a binodal (4,6)-connected topology with the Schläfli symbol of $\{3^2.4^4.5^4.6^4.7\}2\{3^2.6^2.7^2\}$ (Figure 1a–c). It contains two-dimensional irregular channels with pore sizes in the range of 3.7 Å to 6.8 Å, as demonstrated by the PLATON software analysis. The open channels are shown in Figure 1d and 1e, with the window sizes of ∼4.0 × 6.8 Å along the $[\bar{1}01]$ direction and ∼3.9 × 5.4 and 4.1 × 6.8 Å along the [001] direction.

The purity of the bulk HOF-5 sample was confirmed by ^{1}H NMR spectroscopy, thermogravimetric analysis (TGA), and powder XRD studies. ^{1}H and ^{13}C NMR spectra of as-synthesized HOF-5 crystals in DMSO-d_6 solution indicate that HOF-5 contains the pure organic linker and DMF, DMSO, and THF molecules (Figure S2). The TGA curve of HOF-5 (Figure S3) shows that the THF, DMF, and DMSO molecules are gradually lost starting from room temperature to 230 °C. The powder XRD pattern of as-synthesized HOF-5 (immersed in its mother liquid) at room temperature matches well with the simulated XRD pattern based on the crystal structure (without considering solvent molecules), in terms of the peak positions, confirming that the powder sample is a single-phase (Figure S4).

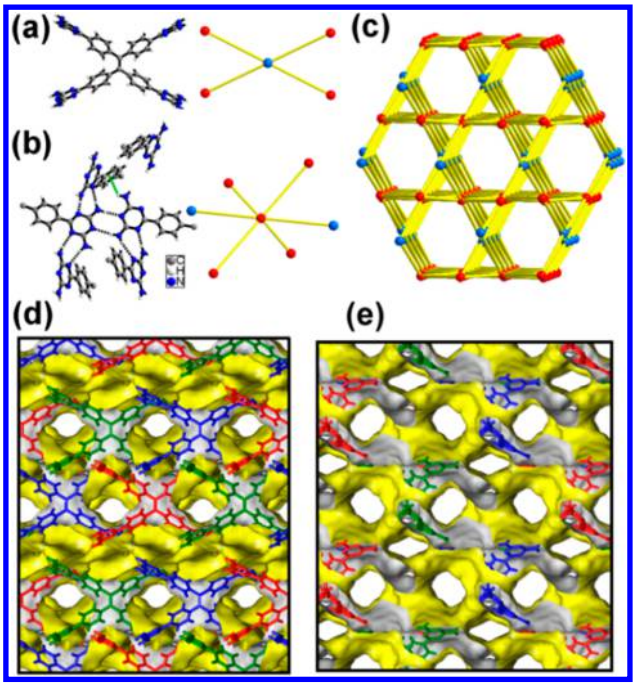

Figure 1. Crystal structure of HOF-5 showing (a) the organic building block acting as a 4-connected node (cyan ball); (b) six neighboring DATs connected through the hydrogen bonding and weak van der Waals interactions [the center acting as a 6-connected node (red ball)]; (c) a binodal (4,6)-connected net; (d and e) packing diagram of HOF-5 along the $[\bar{1}01]$ and [001] direction, respectively, showing the pore surfaces of 2D channels highlighted as yellow/gray (inner/outer) curved planes with pore sizes of (d) ∼4.0 × 6.8 Å and (e) ∼3.9 × 5.4 and 4.1 × 6.8 Å.

Crystal Structure of HOF-5a. Before the gas sorption measurement, the acetone-exchanged crystals of HOF-5 were activated in high vacuum at room temperature to generate activated HOF-5a. During the transition, it was found that the pale-yellowish single crystals of HOF-5 were changed into a light yellow crystalline material, HOF-5a (Figure S5). The flexible nature of HOF-5 is indicated by powder XRD patterns of HOF-5 and HOF-5a (Figure S6), which motivated us to further investigate the structure of activated HOF-5a and their framework transformation during the activation. The structure of HOF-5a was solved using the direct method, and Rietveld refinement was performed on the powder XRD data (see Figure S7). Activated HOF-5a crystallizes in space group *C*2/*m*. Each organic linker in HOF-5a is still linked by eight organic linkers but via 24 hydrogen bonds between DATs (20 hydrogen bonds in HOF-5). The hydrogen bonding interactions in HOF-5a are apparently strengthened, as demonstrated in the shorter D···A distances and angles of D-H···A much closer to 180° (Table 2), which stabilizes the activated framework. HOF-5a retains the same framework connectivity and topology of HOF-5 as a binodal (4,6)-

DOI: 10.1021/jacs.5b05644
J. Am. Chem. Soc. 2015, 137, 9963–9970

Table 2. Comparison of the Hydrogen Bonding Interactions and Close Contact in the Crystal Structures of HOF-5 and HOF-5a

D−H···A	distance of D···A (Å)	angle of D−H···A (deg)
HOF-5		
N4−H4A···N7#1	2.924(4)	175.8
N4−H4B···N6#2	2.986(4)	176.3
N5−H5B···N3#3	3.030(5)	153.8
N9−H9A···N2#4	3.193(4)	166.8
N9−H9B···N1#2	3.385(4)	160.5
N10−H10B···N8#3[a]	5.394(2)	152.6
HOF-5a		
N19−H16···N22#1	2.966(5)	173.2
N19−H17···N20#2	3.011(1)	175.7
N18−H15···N21#3	2.920(8)	170.6
N19−H16···N22#1	2.966(5)	173.2
N19−H17···N20#2	3.011(1)	175.7
N18−H15···N21#3	2.920(8)	170.6

[a]Close contact among DATs for HOF-5. Symmetric code for HOF-5, #1: 1.5 − *x*, 0.5 + *y*, 1.5 − *z*, #2: 1.5 − *x*, 1.5 − *y*, 1 − *z*, #3: 1 − *x*, *y*, 1.5 − *z*, #4: 1.5 − *x*, −0.5 + *y*, 1.5 − *z*. For HOF-5a, #1: 1.5 − *x*, 0.5 − *y*, 1 − *z*, #2: 1 − *x*, *y*, 1 − *z*, #3: 1 − *x*, *y*, −*z*.

connected net with the Schläfli symbol of $\{3^2.4^4.5^4.6^4.7\}2\{3^2.6^2.7^2\}$ (Figure 2a and 2b).

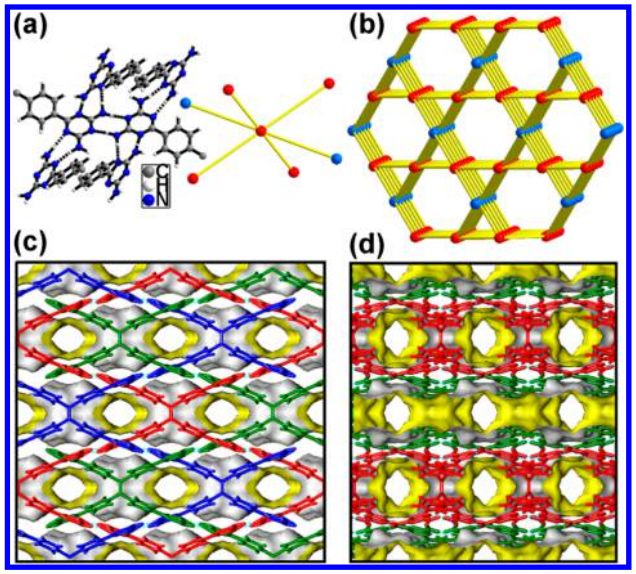

Figure 2. Crystal structure of HOF-5a indicating (a) multiple hydrogen bonding interactions between neighboring six DAT groups [their center acting as a 6-connected node (red balls), while the center of each organic linker acting as a 4-connected node (cyan ball)]; (b) a binodal (4,6)-connected hydrogen-bonded organic framework net; (c and d) packing diagram along the [001] and [100] directions, respectively, showing the pore surfaces of 2D channels highlighted as yellow/gray (inner/outer) curved planes with pore sizes of (c) ~3.9 × 6.8 Å and (d) ~3.9 × 5.5 Å.

The framework quite significantly contracts after solvent removal. As shown in Table 1, the unit cell volume changes from 6769.1 Å^3 (Z = 4) in HOF-5 to 2675.0 Å^3 (Z = 2) in HOF-5a with ~21% framework contraction. Accordingly, HOF-5a has less solvent-accessible void space (41.1%) than that for HOF-5 (55.3%). More specifically, the supramolecular grid of ~22.5 × 34.7 Å in HOF-5 contracts to ~17.8 × 36.5 Å in HOF-5a (Figure S1). The neighboring layers slip slightly with respect to each other as well (Figure S8). The 2D pore channels in HOF-5a are more ordered and slightly smaller than those in HOF-5. They are ~3.9 × 6.8 Å along the [001] direction (Figure 2c) and ~3.9 × 5.5 Å along the [100] direction (Figure 2d). We point out that, in comparison with other HOFs containing DAT moieties (which usually collapses after removal of guests), all amino groups of HOF-5a utilized to support the hydrogen-bonded organic channels should be responsible for the permanent porosity. In addition, HOF-5 can be basically recovered from HOF-5a by immersing it into dry acetone, as indicated by the powder XRD patterns (Figure S9). Then the acetone-regenerated sample can be subsequently activated again to reproduce HOF-5a. We repeated the cycling process three times, and the powder XRD patterns of HOF-5a remain nearly unchanged (Figure S9), suggesting good reversibility between HOF-5 and HOF-5a.

Establishment of Permanent Porosity. The porous nature of HOF-5a, as revealed by its crystal structure, encouraged us to examine its permanent porosity through the gas sorption studies. HOF-5a displays stepwise N_2 adsorption and desorption isotherms at 77 K, with a narrow hysteresis loop (Figure 3). Such stepwise N_2 gas sorption isotherms have been

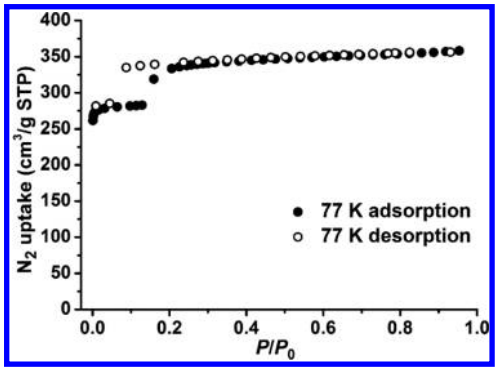

Figure 3. N_2 adsorption/desorption isotherms of HOF-5a.

found in many well-known flexible MOFs, but have not been previously observed in porous HOFs. The unique sorption behaviors indicate that HOF-5a exhibits a flexible robust (porous) framework. The BET surface area of HOF-5a derived from the N_2 isotherm is 1101 m^2/g (Figure S10). The experimental pore volume of HOF-5a is 0.44 cm^3/g, corresponding to the first step N_2 adsorption isotherm at 77 K, recorded at P/P_0 = 0.13. This value matches well with the calculated value of 0.43 cm^3/g for HOF-5a deduced from the crystal structure. In addition, the total pore volume is 0.55 cm^3/g based on the N_2 uptake at P/P_0 = 0.96, which is lower than the theoretical pore volume (0.72 cm^3/g) from the crystal structure of HOF-5 (without considering the solvent molecules), suggesting that HOF-5a has not been fully expanded back to HOF-5 under this sorption condition.

Gas Sorption. Single-component gas sorption isotherms recorded on HOF-5a at two different temperatures are presented in Figure 4a and 4b. The adsorption isotherm for C_2H_2 measured at 296 K shows that HOF-5a adsorbs a relatively high amount of C_2H_2 with an uptake of 101.7 cm^3/g (STP) at 1 atm. This is the highest C_2H_2 uptake among all reported HOFs (Table 3). At 273 K, a stepwise adsorption isotherm of C_2H_2 is observed as well because of the framework flexibility. Its C_2H_2 uptake at 1 atm is 182.0 cm^3/g (173.8 cm^3/

DOI: 10.1021/jacs.5b05644
J. Am. Chem. Soc. 2015, 137, 9963−9970

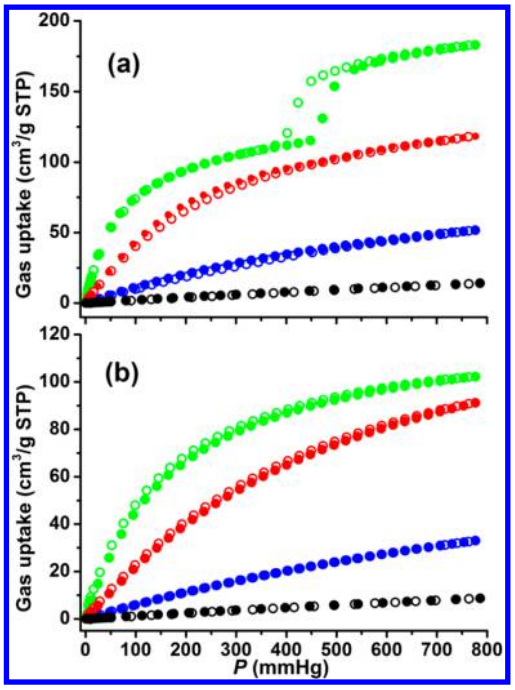

Figure 4. C_2H_2, CO_2, CH_4, and N_2 sorption isotherms (a) at 273 K and (b) at 296 K (C_2H_2: green, CO_2: red, CH_4: blue, N_2: black, solid symbols: adsorption, open symbols: desorption).

cm^3), which is not only the highest among all HOFs so far, but also comparable to those few MOFs with high acetylene storage capacities.[21]

CO_2 uptakes of HOF-5a at 273 and 296 K (1 atm) are 117.1 cm^3/g (111.8 cm^3/cm^3) and 90.0 cm^3/g (86.0 cm^3/cm^3), respectively, demonstrating HOF-5a as the best HOF material for potential carbon dioxide capture and separation. Its carbon dioxide capture capacities are even comparable to one of the best MOFs, HKUST-1 $Cu_3(BTC)_2$.[22] As expected, HOF-5a (under 1 atm) takes up much less methane 50.9 cm^3/g at 273 K; 32.0 cm^3/g at 296 K and nitrogen 13.4 cm^3/g at 273 K; 8.2 cm^3/g at 296 K under 1 atm.

The coverage-dependent adsorption enthalpies of HOF-5a to C_2H_2, CO_2, C_2H_4, and N_2 were calculated using their adsorption isotherms at 273 and 296 K according to the virial method (Figure S11). The enthalpies at zero coverage are 27.6, 22.8, 19.2, and 14.1 kJ/mol for C_2H_2, CO_2, CH_4, and N_2, respectively, which confirms the gas affinity in the order of C_2H_2 > CO_2 > CH_4 > N_2.

We further examined the potential of HOF-5a for gas separations. The mixture selectivities at different pressures and temperatures were calculated based on the well-known ideal adsorbed solution theory (IAST) for mixed C_2H_2/CH_4 (50:50), CO_2/CH_4 (50:50), and CO_2/N_2 (10:90) (Figures 5 and S12–S14 and Table S2). The C_2H_2/CH_4 and CO_2/CH_4 molar selectivities for HOF-5a have been predicted to be 13.6 and 5.0, respectively, at 296 K and 1 atm. CO_2/N_2 selectivity for a 10:90 mixture, a mimic composition in postcombustion carbon dioxide capture, is 22.4 at 296 K and 1 atm. It needs to be pointed out that HOF-5a not only has the highest CO_2 capture amount among the reported HOFs, but also displays a high CO_2/N_2 selectivity,[8,9] underlying the uniqueness of this new HOF for carbon dioxide capture and separation.

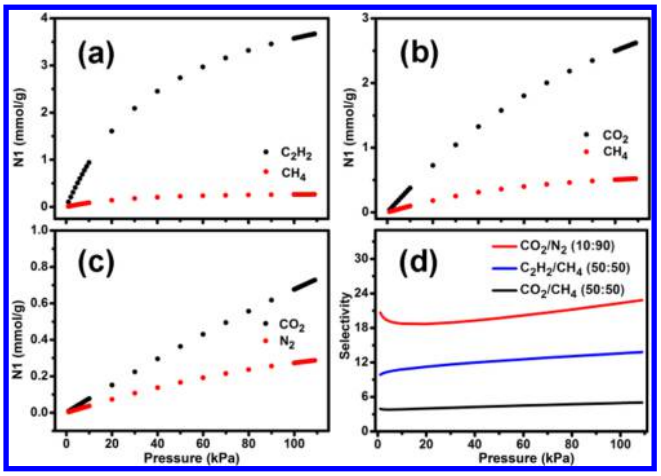

Figure 5. Mixture adsorption isotherms (a–c) and gas selectivities (d) of HOF-5a at 296 K predicted by IAST for C_2H_2/CH_4 (50:50), CO_2/CH_4 (50:50), and CO_2/N_2 (10:90).

Binding Sites within HOF-5a for Carbon Dioxide Capture. The CO_2 uptake at 296 K corresponds to ~3.1 mol of CO_2 adsorbed per mole of HOF-5a. To probe the CO_2 preferential adsorption sites, neutron diffraction measurement was performed. The data of HOF-5a loaded with ~1.5CO_2 per organic linker molecule (HOF-5a ⊃ 1.5CO_2) are shown in Figure 6 along with Rietveld structural refinement. Two

Table 3. Comparison of BET Surface Area, Acetylene Uptake, and Carbon Dioxide Uptake in Reported HOFs

HOFs	BET S_A (m^2/g)	C_2H_2 (cm^3/g)		CO_2 (cm^3/g)		framework density (g/cm^3)[e]	ref
		273 K	296 K	273 K	296 K		
$Ni(tame)_2(PES)_2$	392[a]	–	–	–	–	–	8a
SOF-1a	474[b]	61	50	30	16	0.931	8b
HOF-8	–	–	–	–	57	1.133	8c
TTBI	2796[a]	–	–	81	–	0.755	8d
SOF-7a	900[c]	–	–	64	33	0.883	8e
TPZ	1159[a]	–	–	–	–	1.059	8f
HOF-1a	359[d]	63	55	–	–	0.835	9a
HOF-2a	238[d]	–	–	–	–	0.883	9b
HOF-3a	165[d]	58	47	31	21	0.430	9c
HOF-4a	312[d]	–	–	–	–	0.899	9d
HOF-5a	1101[a]	182	102	117	90	0.955	this work

[a]Determined from N_2 isotherm at 77 K. [b]Calculated from N_2 adsorption at 125 K. [c]Deduced from CO_2 adsorption at 273 K. [d]Determined from CO_2 adsorption at 196 K. [e]Calculation based on the crystal data without consideration of solvent molecules.

DOI: 10.1021/jacs.5b05644
J. Am. Chem. Soc. 2015, 137, 9963–9970

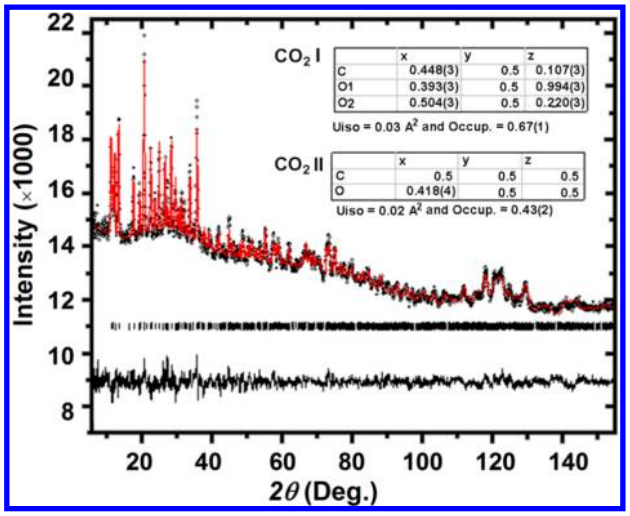

Figure 6. Experimental (circles), calculated (line), and difference (line below observed and calculated patterns) powder neutron diffraction profiles for HOF-5a loaded with CO_2 measured at 200 K. CO_2 molecules were kept as rigid bodies during the Rietveld structural refinement. Vertical bars indicate the calculated positions of Bragg peaks. Goodness of fit data: R_{wp} = 0.0123, R_p = 0.0093, χ^2 = 1.42. The refined gas molecule coordinates are shown in the inset.

primary CO_2 adsorption sites were identified from the data. The refined CO_2 concentration is ~1.44CO_2 per organic linker molecule, consistent with the experimental amount of gas (~1.5CO_2 per L molecule) loaded into the material. Figure 7a and b show the preferential CO_2 binding positions (sites I and II) and orientations. The CO_2 molecules are located on these sites filling in the cavities along the [001] direction. Full occupancy of the two CO_2 sites identified from neutron diffraction (3 mol of CO_2 per mol of HOF-5a) would largely account for the CO_2 uptake at 296 K and 1 atm (~3.1 mol of CO_2 per mol of HOF-5a) as observed in the adsorption isotherm.

To evaluate the CO_2 adsorption energetics in HOF-5a, we performed dispersion-corrected density functional theory (DFT-D) calculations.[19,20] The DFT-D optimized CO_2 adsorption configurations (see Table S3) are in excellent agreement with the experimental results, strongly corroborating our structural analysis of the neutron diffraction data. The calculated static CO_2 binding energies are 39.9 and 37.3 kJ/mol for the two respective CO_2 adsorption sites. This small difference in binding energies on these two energetically favored sites is in line with the fact that these two sites get populated simultaneously with different occupancies as indicated in the diffraction data.

In the present case, the expected strong hydrogen bonds between the CO_2 molecules and DAT moieties were not observed since all amino groups were utilized to support the hydrogen-bonded organic channels of HOF-5a. The carbon dioxide interactions with the hydrogen-bonded organic framework are mainly of van der Waals nature. The moderately strong host−guest interaction is indicated by the nearest distance of 3.36 Å between the C atom of carbon dioxide (site I) and the N atom in HOF-5a (Figure 7a).[23] For site II, the CO_2 molecule interacts with HOF-5a via the C−H···O interaction, as implied by the short H···O distance of 2.80 Å. In addition, two kinds of weak interactions between neighboring carbon dioxide molecules are suggested in terms of the short C···O separation of 3.45 Å for adjacent carbon

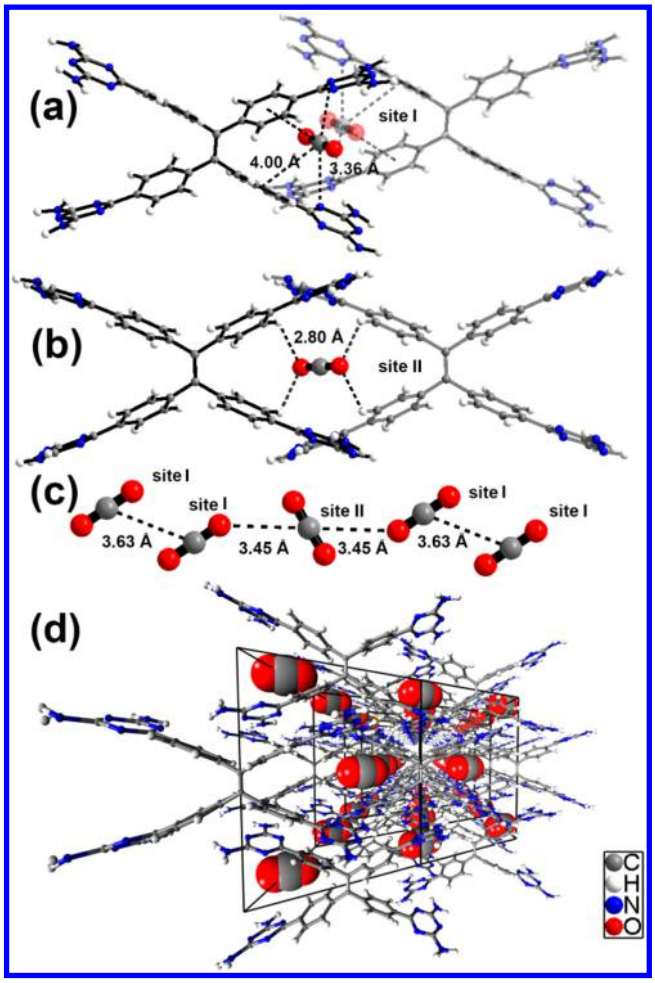

Figure 7. Neutron diffraction crystal structure of HOF-5a ⊃ 1.5CO_2 showing (a and b) preferential binding sites for CO_2 uptake (sites I and II) and their close contacts with the framework fragments; (c) weak interactions among CO_2 molecules located at binding sites I and II to form a pseudo-one-dimensional array; (d) packing diagram illustrating the high density of adsorbed CO_2 molecules.

dioxide molecules (one on site I and the other on site II) as well as the C···C separation of 3.63 Å between adjacent CO_2 (both on site I), which links those CO_2 molecules into pseudo-one-dimensional arrays (Figure 7b and 7c) along the [001] direction, and largely contributes to the high density of adsorbed CO_2 molecules in HOF-5a. The unique pore structure with suitable pore sizes, curvatures, and functional sites has enabled HOF-5a to take up a large amount of CO_2 molecules.

■ CONCLUSIONS

In summary, we have realized the first example of a highly porous (robust) and flexible hydrogen-bonded organic framework (HOF-5), exhibiting a significant framework contraction of ~21% with respect to the activated species. Compared with those developed HOFs with less porosities before,[9] not only does this HOF have multiple DAT moieties, but also more importantly, these DAT moieties are oriented in a way to enforce a large number of strong hydrogen bonding interactions (each organic linker in HOF-5a is linked by eight organic linkers but via 24 hydrogen bonds between DATs), thus stabilizing the framework. The suitable pore sizes, curvatures, and functional sites on the pore surfaces enable

DOI: 10.1021/jacs.5b05644
J. Am. Chem. Soc. 2015, 137, 9963−9970

this HOF to take up a large amount of carbon dioxide molecules (the highest carbon dioxide uptake among reported HOFs), which has been revealed in the sorption isotherms, neutron powder diffraction studies, and theoretical calculations. This work not only demonstrates the uniqueness of HOFs, but also establishes some common features between MOFs and HOFs. We hope that these findings stimulate more extensive research on HOFs in both the chemistry and materials science communities.

■ ASSOCIATED CONTENT

Supporting Information

Supramolecular structures of HOF-5 and HOF-5a, photographs of as-synthesized HOF-5 and HOF-5a, powder XRD patterns of HOF-5 and HOF-5a, TGA curve of HOF-5, mixture adsorption isotherms and selectivities of CO_2/CH_4 (50:50) and CO_2/N_2 (10:90) predicted by IAST at 273 K. (PDF). X-ray crystallographic data for HOF-5. (CIF). X-ray crystallographic data for HOF-5a. (CIF). The Supporting Information is available free of charge on the ACS Publications website at DOI: 10.1021/jacs.5b05644.

■ AUTHOR INFORMATION

Corresponding Authors

*wzhou@nist.gov

*banglin.chen@utsa.edu

Notes

The authors declare no competing financial interest.

■ ACKNOWLEDGMENTS

This work was supported by the grant AX-1730 from the Welch Foundation (B.C.).

■ REFERENCES

(1) (a) Yu, J.; Xu, R. *Acc. Chem. Res.* **2010**, *43*, 1195. (b) Linares, N.; Silvestre-Albero, A. M.; Serrano, E.; Silvestre-Albero, J.; García-Martínez, J. *Chem. Soc. Rev.* **2014**, *43*, 7681. (c) Roth, W. J.; Nachtigall, P.; Morris, R. E.; Čejka, J. *Chem. Rev.* **2014**, *114*, 4807.

(2) (a) Zhao, D.; Feng, J.; Huo, Q.; Melosh, N.; Frederickson, G. H.; Chmelka, B. F.; Stucky, G. D. *Science* **1998**, *279*, 548. (b) Davis, M. E. *Acc. Chem. Res.* **1993**, *26*, 111. (c) Valtchev, V.; Tosheva, L. *Chem. Rev.* **2013**, *113*, 6734. (d) Navalon, S.; Dhakshinamoorthy, A.; Alvaro, M.; Garcia, H. *Chem. Rev.* **2014**, *114*, 6179. (e) Yue, Y.; Mayes, R. T.; Kim, J.; Fulvio, P. F.; Sun, X.-G.; Tsouris, C.; Chen, J.; Brown, S.; Dai, S. *Angew. Chem., Int. Ed.* **2013**, *52*, 13458.

(3) (a) Furukawa, H.; Cordova, K. E.; O'Keeffe, M.; Yaghi, O. M. *Science* **2013**, *341*, 974. (b) Zhang, J.-P.; Zhang, Y.-B.; Lin, J.-B.; Chen, X.-M. *Chem. Rev.* **2012**, *112*, 1001. (c) Sato, H.; Kosaka, W.; Matsuda, R.; Hori, A.; Hijikata, Y.; Belosludov, R. V.; Sakaki, S.; Takata, M.; Kitagawa, S. *Science* **2014**, *343*, 167. (d) Li, J.-R.; Sculley, J.; Zhou, H.-C. *Chem. Rev.* **2012**, *112*, 869. (e) Zhu, Q.-L.; Xu, Q. *Chem. Soc. Rev.* **2014**, *43*, 5468. (f) Eddaoudi, M.; Sava, D. F.; Eubank, J. F.; Adil, K.; Guillerm, V. *Chem. Soc. Rev.* **2015**, *44*, 228. (g) Cui, Y.; Yue, Y.; Qian, G.; Chen, B. *Chem. Rev.* **2012**, *112*, 1126. (h) Chen, B.; Xiang, S.; Qian, G. *Acc. Chem. Res.* **2010**, *43*, 1115. (i) Zhao, X.; Bu, X.; Zhai, Q.-G.; Tran, H.; Feng, P. *J. Am. Chem. Soc.* **2015**, *137*, 1396.

(4) (a) Vaidhyanathan, R.; Iremonger, S. S.; Shimizu, G. K. H.; Boyd, P. G.; Alavi, S.; Woo, T. K. *Science* **2010**, *330*, 650. (b) Serre, C.; Mellot-Draznieks, C.; Surblé, S.; Audebrand, N.; Filinchuk, Y.; Férey, G. *Science* **2007**, *315*, 1828. (c) Zhang, Z.; Zaworotko, M. J. *Chem. Soc. Rev.* **2014**, *43*, 5444. (d) Wu, H.; Gong, Q.; Olson, D. H.; Li, J. *Chem. Rev.* **2012**, *112*, 836. (e) Gao, W.-Y.; Chrzanowski, M.; Ma, S. *Chem. Soc. Rev.* **2014**, *43*, 5841. (f) Li, T.; Kozlowski, M. T.; Doud, E. A.; Blakely, M. N.; Rosi, N. L. *J. Am. Chem. Soc.* **2013**, *135*, 11688. (g) Chen, L.; Reiss, P. S.; Chong, S. Y.; Holden, D.; Jelfs, K. E.; Hasell, T.; Little, M. A.; Kewley, A.; Briggs, M. E.; Stephenson, A.; Thomas, K. M.; Armstrong, J. A.; Bell, J.; Busto, J.; Noel, R.; Liu, J.; Strachan, D. M.; Thallapally, P. K.; Cooper, A. I. *Nat. Mater.* **2014**, *13*, 954. (h) Wang, C.; Zhang, T.; Lin, W. *Chem. Rev.* **2012**, *112*, 1084. (i) Farha, O. K.; Yazaydin, O.; Eryazici, I.; Malliakas, C.; Hauser, B.; Kanatzidis, M. G.; Nguyen, S. T.; Snurr, R. Q.; Hupp, J. T. *Nat. Chem.* **2010**, *2*, 944. (j) Wang, Z.; Cohen, S. M. *Chem. Soc. Rev.* **2009**, *38*, 1315. (k) Wu, H.; Chua, Y. S.; Krungleviciute, V.; Tyagi, M.; Chen, P.; Yildirim, T.; Zhou, W. *J. Am. Chem. Soc.* **2013**, *135*, 10525.

(5) (a) Doonan, C. J.; Tranchemontagne, D. J.; Glover, T. G.; Hunt, J. R.; Yaghi, O. M. *Nat. Chem.* **2010**, *2*, 235. (b) Xu, Y.-H.; Jin, S.-B.; Xu, H.; Nagai, A.; Jiang, D.-L. *Chem. Soc. Rev.* **2013**, *42*, 8012.

(6) (a) Wuest, J. D. *Chem. Commun.* **2005**, 5830. (b) Simard, M.; Wuest, J. D. *J. Am. Chem. Soc.* **1991**, *113*, 4696. (c) Tian, J.; Thallapally, P. K.; McGrail, B. P. *CrystEngComm* **2012**, *14*, 1909. (d) McKeown, N. B. *J. Mater. Chem.* **2010**, *20*, 10588. (e) Kolotuchin, S. V.; Fenlon, E. E.; Wilson, S. R.; Loweth, C. J.; Zimmerman, S. C. *Angew. Chem., Int. Ed. Engl.* **1995**, *34*, 2654.

(7) (a) Endo, K.; Sawaki, T.; Koyanagi, M.; Kobayashi, K.; Masuda, H.; Aoyama, Y. *J. Am. Chem. Soc.* **1995**, *117*, 8341. (b) Brunet, P.; Simard, M.; Wuest, J. D. *J. Am. Chem. Soc.* **1997**, *119*, 2737. (c) Holman, K. T.; Pivovar, A. M.; Swift, J. A.; Ward, M. D. *Acc. Chem. Res.* **2001**, *34*, 107. (d) Saied, O.; Maris, T.; Wuest, J. D. *J. Am. Chem. Soc.* **2003**, *125*, 14956. (e) Kobayashi, K.; Sato, A.; Sakamoto, S.; Yamaguchi, K. *J. Am. Chem. Soc.* **2003**, *125*, 3035. (f) Malek, N.; Maris, T.; Perron, M.; Wuest, J. D. *Angew. Chem., Int. Ed.* **2005**, *44*, 4021. (g) Maly, K. E.; Gagnon, E.; Maris, T.; Wuest, J. D. *J. Am. Chem. Soc.* **2007**, *129*, 4306. (h) Liu, Y.; Hu, C.; Comotti, A.; Ward, M. D. *Science* **2011**, *333*, 436. (i) Yamamoto, A.; Hamada, T.; Hisaki, I.; Miyata, M.; Tohna, N. *Angew. Chem., Int. Ed.* **2013**, *52*, 1709. (j) Xiao, W.; Hu, C.; Ward, M. D. *J. Am. Chem. Soc.* **2014**, *136*, 14200. (k) Reddy, D. S.; Duan, S.; Shimizu, G. K. H. *Angew. Chem., Int. Ed.* **2003**, *42*, 1360. (l) Görbitz, C. H. *Chem. - Eur. J.* **2001**, *7*, 5153. (m) Görbitz, C. H. *Chem. - Eur. J.* **2007**, *13*, 1022. (n) Soldatov, D. V.; Moudrakovski, I. L.; Grachev, E. V.; Ripmeester, J. A. *J. Am. Chem. Soc.* **2006**, *128*, 6737. (o) Natarajan, R.; Magro, G.; Bridgland, L. N.; Sirikulkajorn, A.; Narayanan, S.; Ryan, L. E.; Haddow, M. F.; Orpen, A. G.; Charmant, J. P. H.; Hudson, A. J.; Davis, A. P. *Angew. Chem., Int. Ed.* **2011**, *50*, 11386.

(8) (a) Dalrymple, S. A.; Shimizu, G. K. H. *J. Am. Chem. Soc.* **2007**, *129*, 12114. (b) Yang, W.; Greenaway, A.; Lin, X.; Matsuda, R.; Blake, A. J.; Wilson, C.; Lewis, W.; Hubberstey, P.; Kitagawa, S.; Champness, N. R.; Schröder, M. *J. Am. Chem. Soc.* **2010**, *132*, 14457. (c) Luo, X.-Z.; Jia, X.-J.; Deng, J.-H.; Zhong, J.-L.; Liu, H.-J.; Wang, K.-J.; Zhong, D.-C. *J. Am. Chem. Soc.* **2013**, *135*, 11684. (d) Mastalerz, M.; Oppel, I. M. *Angew. Chem., Int. Ed.* **2012**, *51*, 5252. (e) Lü, J.; Perez-Krap, C.; Suyetin, M.; Alsmail, N. H.; Yan, Y.; Yang, S.; Lewis, W.; Bichoutskaia, E.; Tang, C. C.; Blake, A. J.; Cao, R.; Schröder, M. *J. Am. Chem. Soc.* **2014**, *136*, 12828. (f) Chen, T.-H.; Popov, I.; Kaveevivitchai, W.; Chuang, Y.-C.; Chen, Y.-S.; Daugulis, O.; Jacobson, A. J.; Miljanić, O. Š. *Nat. Commun.* **2014**, *5*, 5131. (g) Dalapati, S.; Saha, R.; Jana, S.; Patra, A. K.; Bhaumik, A.; Kumar, S.; Guchhait, N. *Angew. Chem., Int. Ed.* **2012**, *51*, 12534. (h) Hisaki, I.; Nakagawa, S.; Tohnai, N.; Miyata, M. *Angew. Chem., Int. Ed.* **2015**, *54*, 3008. (i) Natarajan, R.; Bridgland, L.; Sirikulkajorn, A.; Lee, J.-H.; Haddow, M. F.; Magro, G.; Ali, B.; Narayanan, S.; Strickland, P.; Charmant, J. P. H.; Orpen, A. G.; McKeown, N. B.; Bezzu, C. G.; Davis, A. P. *J. Am. Chem. Soc.* **2013**, *135*, 16912. (j) Soldatov, D. V.; Moudrakovski, I. L.; Ripmeester, J. A. *Angew. Chem., Int. Ed.* **2004**, *43*, 6308. (k) Thallapally, P. K.; McGrail, B. P.; Atwood, J. L.; Gaeta, C.; Tedesco, C.; Neri, P. *Chem. Mater.* **2007**, *19*, 3354. (l) Tian, J.; Thallapally, P. K.; Dalgarno, S. J.; Atwood, J. L. *J. Am. Chem. Soc.* **2009**, *131*, 13216. (m) Afonso, R. V.; Durão, J.; Mendes, A.; Damas, A. M.; Gales, L. *Angew. Chem., Int. Ed.* **2010**, *49*, 3034.

(9) (a) He, Y.; Xiang, S.; Chen, B. *J. Am. Chem. Soc.* **2011**, *133*, 14570. (b) Li, P.; He, Y.; Zhao, Y.; Weng, L.; Wang, H.; Krishna, R.; Wu, H.; Zhou, W.; O'Keeffe, M.; Han, Y.; Chen, B. *Angew. Chem., Int. Ed.* **2015**, *54*, 574. (c) Li, P.; He, Y.; Arman, H. D.; Krishna, R.; Wang, H.; Weng, L.; Chen, B. *Chem. Commun.* **2014**, *50*, 13081. (d) Li, P.;

DOI: 10.1021/jacs.5b05644
J. Am. Chem. Soc. 2015, 137, 9963−9970

He, Y.; Guang, J.; Weng, L.; Zhao, J. C.-G.; Xiang, S.; Chen, B. *J. Am. Chem. Soc.* **2014**, *136*, 547. (e) Yang, W.; Li, B.; Wang, H.; Alduhaish, O.; Alfooty, K.; Aldin Zayed, M.; Li, P.; Arman, H. D.; Chen, B. *Cryst. Growth Des.* **2015**, *15*, 2000.
(10) Li, R.; Hu, W.; Liu, Y.; Zhu, D. *Acc. Chem. Res.* **2010**, *43*, 529.
(11) Buckles, R. E.; Hausman, E. A.; Wheeler, N. G. *J. Am. Chem. Soc.* **1950**, *72*, 2494.
(12) Bhunia, A.; Vasylyeva, V.; Janiak, C. *Chem. Commun.* **2013**, *49*, 3961.
(13) Sun, Z.; Li, Y.; Chen, L.; Jing, X.; Xie, Z. *Cryst. Growth Des.* **2015**, *15*, 542.
(14) Myers, A. L.; Prausnitz, J. M. *AIChE J.* **1965**, *11*, 121.
(15) Li, B.; Zhang, Y.; Krishna, R.; Yao, K.; Han, Y.; Wu, Z.; Ma, D.; Shi, Z.; Pham, T.; Space, B.; Liu, J.; Thallapally, P. K.; Liu, J.; Chrzanowski, M.; Ma, S. *J. Am. Chem. Soc.* **2014**, *136*, 8654.
(16) Sheldrick, G. M. *Acta Crystallogr., Sect. A: Found. Crystallogr.* **2008**, *A64*, 112.
(17) Spek, A. L. *PLATON, A Multipurpose Crystallographic Tool*; Utrecht University: Utrecht, the Netherlands, 2005.
(18) Larson, A. C.; Von Dreele, R. B. *General Structure Analysis System*, Report LAUR 86−748; Los Alamos National Laboratory: Los Alamos, NM, 1994.
(19) Giannozzi, P.; Baroni, S.; Bonini, N.; Calandra, M.; Car, R.; Cavazzoni, C.; Ceresoli, D.; Chiarotti, G. L.; Cococcioni, M.; Dabo, I.; Dal Corso, A.; Fabris, S.; Fratesi, G.; de Gironcoli, S.; Gebauer, R.; Gerstmann, U.; Gougoussis, C.; Kokalj, A.; Lazzeri, M.; Martin-Samos, L.; Marzari, N.; Mauri, F.; Mazzarello, R.; Paolini, S.; Pasquarello, A.; Paulatto, L.; Sbraccia, C.; Scandolo, S.; Sclauzero, G.; Seitsonen, A. P.; Smogunov, A.; Umari, P.; Wentzcovitch, R. M. *J. Phys.: Condens. Matter* **2009**, *21*, 395502.
(20) Barone, V.; Casarin, M.; Forrer, D.; Pavone, M.; Sambi, M.; Vittadini, A. *J. Comput. Chem.* **2009**, *30*, 934.
(21) (a) Xiang, S.; Zhou, W.; Gallegos, J. M.; Liu, Y.; Chen, B. *J. Am. Chem. Soc.* **2009**, *131*, 12415. (b) He, Y.; Krishna, R.; Chen, B. *Energy Environ. Sci.* **2012**, *5*, 9107.
(22) (a) Sumida, K.; Rogow, D. L.; Mason, J. A.; McDonald, T. M.; Bloch, E. D.; Herm, Z. R.; Bae, T.-H.; Long, J. R. *Chem. Rev.* **2012**, *112*, 724. (b) Zhang, Z.; Yao, Z.-Z.; Xiang, S.; Chen, B. *Energy Environ. Sci.* **2014**, *7*, 2868.
(23) Liao, P.-Q.; Zhou, D.-D.; Zhu, A.-X.; Jiang, L.; Lin, R.-B.; Zhang, J.-P.; Chen, X.-M. *J. Am. Chem. Soc.* **2012**, *134*, 17380.

DOI: 10.1021/jacs.5b05644
J. Am. Chem. Soc. 2015, 137, 9963−9970